PAPER

Check for updates

Growth regulation of an easily crystallized organic long-persistent luminescence system with *in situ* anti-counterfeiting applications†

Duo Liu,[a] Yakun Song, [ID] *[a] Hao Wang,[a] Tiantian Wang,[b] Zhiyong Zhou,[a] Zhen Liu, [ID] [a] Weiwei Lu[a] and Tianyang Wang [ID] *[b]

Organic long-persistent luminescence (OLPL) materials present significant promise in anti-counterfeiting and information encryption due to their straightforward preparation process and adjustable luminescence properties. In this study, we present a novel approach to the growth regulation of OLPL systems, focusing on an easily crystallizable doping system for *in situ* anti-counterfeiting applications. Utilizing *p*-TPD as the guest molecule and various host molecules, we synthesized doped crystals with uniform particle size and afterglow durations ranging from 2.0 s to 4.5 s. Furthermore, leveraging the unique host–guest pairing relationship and facile crystallization characteristics, we developed a ''paper-ink'' encryption strategy with *in situ* anti-counterfeiting capabilities. This innovative approach allows encrypted paper and paired ink to fully display encrypted information, while ordinary paper treated with the ink remains blank unless further processed with an information display reagent. Notably, the encrypted paper maintains its encryption effectiveness even when exposed to water. These advancements underscore the potential of organic-doped long afterglow materials in enhancing information security for secure communication and data protection.

[a] *School of Chemistry and Chemical Engineering, Henan University of Science and Technology, Luoyang, 471023, China. E-mail: songyakun@haust.edu.cn*

[b] *Key Laboratory of Organic Integrated Circuits, Ministry of Education & Tianjin Key Laboratory of Molecular Optoelectronic Science, Department of Chemistry, School of Science, Tianjin University, Tianjin 300072, China.
E-mail: tianyangwang@tju.edu.cn*

† Electronic supplementary information (ESI) available. See DOI: https://doi.org/10.1039/d4tc01747a

Tianyang Wang is a full professor in the Department of Chemistry, School of Science, Tianjin University. He received his PhD from Tianjin University in 2014. He subsequently joined Prof. Wenping Hu's group as a postdoctoral fellow in the Department of Chemistry at Tianjin University from 2014 to 2017. His research interests focus on the preparation and application of organic long-persistent luminescence materials and organic flexible materials.

Tianyang Wang

1. Introduction

Organic long-persistent luminescence (OLPL) materials are distinguished by their remarkable long afterglow performance, attributable to their unique light storage and slow-release properties. These materials can continue emitting light even after the cessation of excitation by an external light source. This feature endows OLPL materials with vast prospects for application across many fields, including anti-counterfeiting,[1–3] encryption,[4–7] and biological imaging.[8,9] At present, researchers have explored many strategies for constructing organic long-persistent luminescent materials, such as polymerization,[9,10] aggregation,[11,12] introduction of heavy atoms,[13,14] host–guest (H–G) doping,[15–18] and multi-component doping.[19–21] Within this broad strategy, the host–guest doping approach is widely studied due to its straightforward and versatile construction. Ideally, host and guest materials should demonstrate suitable energy level matching to enable charge injection and capture, leading to the formation of stable charge-separated (CS) states with excitons for efficient long-persistent luminescence.[22–24]

At present, the rapid preparation of host–guest doped crystals mainly relies on host molecules that are easy to crystallize.[25,26] Meanwhile, the host molecule can isolate oxygen and restrict non-radiative transitions of excited state electrons, playing an important role in constructing host–guest doping systems.[27,28]

Common host molecules with good crystallinity include diphenylamine,[29] triphenylamine,[30] and triphenylphosphine.[2] These host molecules can quickly form doped crystals with suitable guest molecules. However, the preparation of host–guest doped crystals currently mainly relies on melting crystallization, natural crystallization in organic solvents, or water-based methods.[31–33] These methods can lead to challenges in controlling crystal size and dispersibility. In subsequent applications, grinding is required, which disrupts the crystal morphology and greatly reduces the luminescence performance of doped crystals. This necessitates the development of rapid methods for preparing well-dispersed organic-doped long-persistent luminescent materials to enhance their practical application.

Organic long afterglow crystal materials have made significant advancements in anti-counterfeiting and information encryption applications within the information technology field, owing to their distinctive photophysical properties.[34,35] Currently, anti-counterfeiting and information encryption applications primarily employ techniques such as screen printing, direct writing or coating. Wang and his team[3,36] constructed several host–guest doping systems around guest molecules containing fluorenyl groups. The OLPL materials, after grinding, were blended with polyvinyl pyrrolidone (PVP) to create a slurry, enabling their application in anti-counterfeiting and information encryption *via* screen printing or coating. Cui *et al.*[37] doped a series of guest molecules into 3-PL to obtain composite materials with different luminescent properties, and prepared the composite materials into suspensions for direct writing, thus realizing information encryption. These methods use screen printing, direct writing or coating to directly apply OLPL materials to ordinary paper. However, although these encryption modes are relatively simple, they also have obvious defects such as poor stability, high environmental impact and low encryption level, and their encryption effects are easy to copy and forge. Consequently, we aim to leverage the unique "H–G" matching mechanism of the doping system. The primary objective is to explore novel processing methods to achieve more sophisticated and efficient information encryption while preserving the structure and properties of long afterglow crystals.

Herein, we employed easily crystallizable host molecules, including triphenylphosphine (TPP), triphenylamine (TPA), diphenylamine (DPA), and phenyl benzoate (PB), along with N,N′-diphenyl-N,N′-bis(4-methylphenyl)-4,4′-biphenyldiamine (p-TPD) as a guest molecule with excellent luminescent potential. By integrating the surfactant, we successfully prepared uniformly dispersed doped crystals of TPP: p-TPD, TPA: p-TPD, DPA: p-TPD, and PB: p-TPD. These crystals exhibited distinct afterglow durations of 4.5 s, 2.0 s, 3.0 s, and 2.2 s, respectively. Furthermore, we introduce a novel "paper-ink" strategy for *in situ* anti-counterfeiting, utilizing the easily crystallizable properties of the doped crystals. This approach not only demonstrates exceptional encryption capabilities, allowing encrypted information to be fully displayed only when paired with the specific ink, but also maintains excellent long-afterglow luminescence performance even when the paper with

encrypted information is immersed in water. By leveraging these innovative strategies, we aim to significantly advance the development of organic doped long afterglow materials for information encryption, potentially transforming their application in the field.

2. Experimental

2.1. Preparation of the doped-crystals

Triphenylphosphine (TPP, 1.31 g) and N,N′-diphenyl-N,N′-bis(4-methylphenyl)-4,4′-biphenyldiamine (p-TPD) (0.026 g) were added to 30 mL of water, followed by the addition of surfactant (hexadecyltrimethylammonium bromide, 0.15 mg). The mixture was heated and stirred for 15 minutes, then gradually cooled to induce crystallization. The solution containing the crystals was filtered, and the precipitate was dried to obtain TPP: p-TPD crystals (0.99 g, 99.0% yield). The doped crystals TPA: p-TPD, DPA: p-TPD and PB: p-TPD were prepared using triphenylamine (TPA), diphenylamine (DPA) and phenyl benzoate (PB), respectively, in place of TPP, following the same procedure.

2.2. Preparation of "paper-ink" encryption system materials

To prepare the encrypted paper, 50.0 mg of p-TPD was thoroughly mixed with 50.0 g of pulp, and the mixture was subjected to suction filtration to form a paper cake. The paper cake was then compacted and dried. For the ink, TPP, PVP, and dichloromethane $(30:10:1)$ were added to a beaker and thoroughly stirred to ensure a homogeneous mixture. The information display reagent was prepared by dissolving 15 mg of p-TPD in 5 mL of methylene chloride.

3. Results and discussion

3.1. Fabrication of OLPL materials

The doped crystals prepared by a water-based method with added surfactant (S–W method) (Fig. 1a and b) exhibit excellent luminescent properties. The afterglow times of the doped crystals TPP: p-TPD, TPA: p-TPD, DPA: p-TPD, and PB: p-TPD are about 4.0 s, 2.0 s, 3.0 s and 1.5 s, respectively (Fig. 1c). From the semi logarithmic graph of the emission attenuation curve of the doped crystal (Fig. 1d), it can be seen that the afterglow times of the doped crystals TPP: p-TPD, TPA: p-TPD, DPA: p-TPD, and PB: p-TPD are 4.5 s, 2.0 s, 3.0 s and 2.2 s respectively, which is basically consistent with the observed afterglow time.

As illustrated in Fig. 1e and Fig. S1 (ESI†), the traditional water-based method yields particles with heterogeneous sizes prone to agglomeration, necessitating grinding prior to application. This grinding process leads to material loss, decreasing yield and increasing costs, which substantially restricts both production and practical applications. Consequently, enhancing the dispersibility of OLPL-doped materials is essential while preserving the eco-friendly benefits of the water-based methods. The OLPL doped crystals prepared with surfactants, as shown in Fig. 1f and Fig. S2 (ESI†), demonstrate uniform particle sizes and smoother surfaces. This uniformity allows for
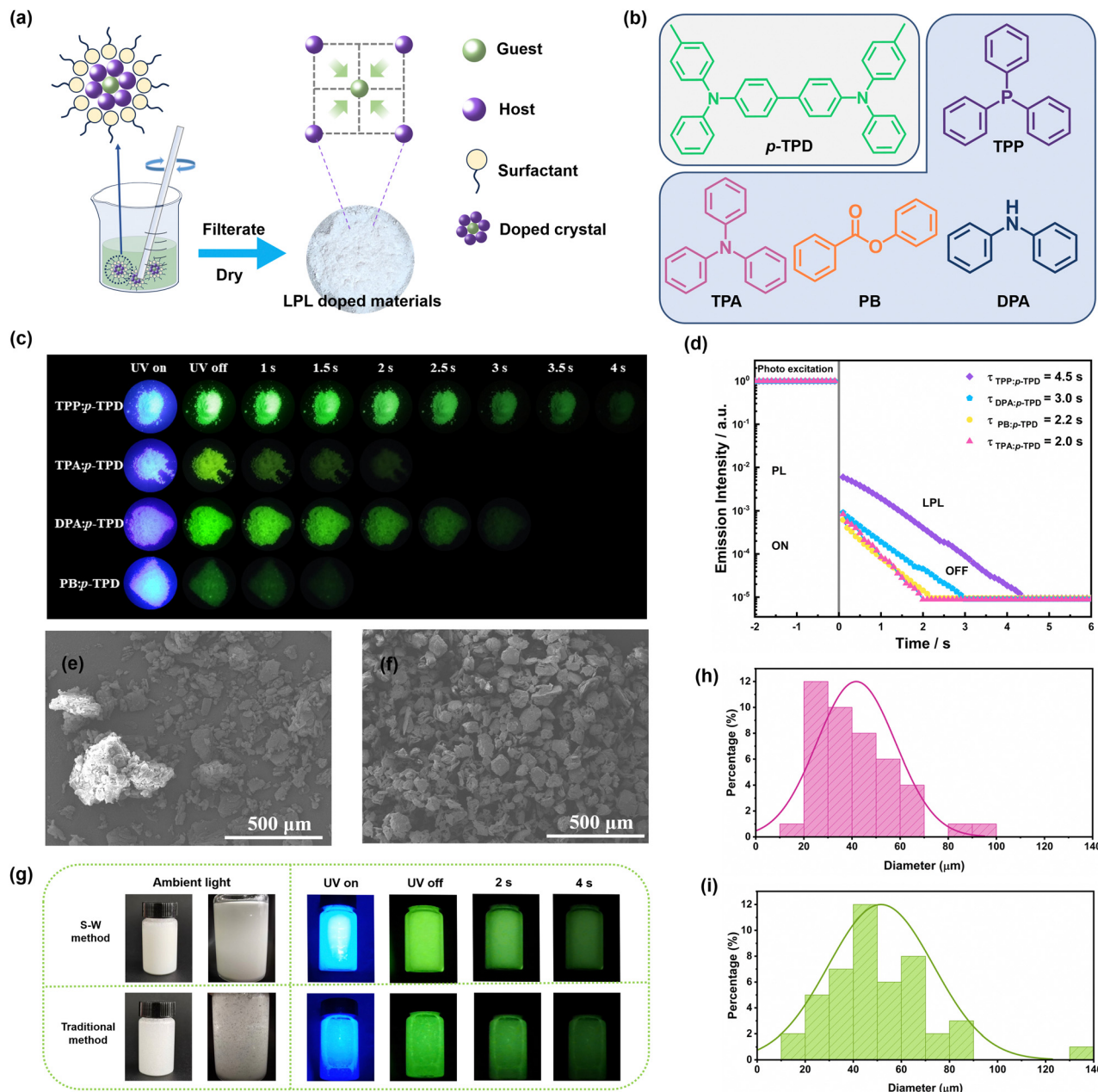
This journal is © The Royal Society of Chemistry 2024

J. Mater. Chem. C, 2024, **12**, 10942–10949 | **10943**

Fig. 1 (a) Preparation process diagram of the OLPL materials. (b) Molecular structure diagrams of *p*-TPD, TPP, TPA, DPA and PB. (c) LPL images of TPP: *p*-TPD, TPA: *p*-TPD, DPA: *p*-TPD, and PB: *p*-TPD under ambient conditions (excitation: 365 nm). (d) Semi-logarithmic plot of the emission decay profile of different OLPL materials (sample-temperature: 300 K; excitation: 365 nm; excitation time: 2 s; excitation power: 10 mW). SEM electron microscopy images of the crystals prepared by the traditional water-based method (e) and S–W method (f). (g) The dispersion and luminescent properties of the crystals prepared by the S–W method and traditional water-based method in PVP aqueous solution. Particle size distribution diagram of the crystals prepared by the S–W method (h) and traditional water-based method (i).

direct application without the need for subsequent grinding, thus preserving the OLPL performance as depicted in Fig. S3 (ESI†). Introducing these unground doped crystals into a PVP aqueous solution (Fig. 1g and Video S1, ESI†) clearly shows that the dispersion of the crystals produced by the S–W method is superior to that of the traditional method, maintaining excellent luminescent properties and uniform glow. The improved dispersibility facilitates the direct use of the crystals in slurry preparation, significantly enhancing their practical production and application potential.

Furthermore, as depicted in Fig. 1h and i, the particle size distribution of OLPL doped crystals prepared with surfactants is predominantly within the 20–70 μm range, indicating uniformity. In contrast, crystals produced by the traditional water-based method show a broader distribution from 10–90 μm and include particles as large as 130–140 μm, signaling severe agglomeration. However, the maximum particle size of materials synthesized *via* the S–W method does not exceed 100 μm, demonstrating effective anti-agglomeration characteristics.

10944 | *J. Mater. Chem. C*, 2024, **12**, 10942–10949

This journal is © The Royal Society of Chemistry 2024

This difference is attributed to the gradual formation of numerous cavity molecules at the hydrophobic ends of the surfactants during continuous stirring in the aqueous solution.[38-41] Within these cavities, host and guest molecules converge, leading to the gradual formation of doped crystals as the temperature decreases. The abundance of cavities significantly enhances the dispersion of doped crystals, thereby resulting in more uniform particle sizes. Moreover, even after filtering and drying, the OLPL doped crystals retain surfactants on their surfaces, which facilitates their complete dispersion in water, making them more suitable for practical application in aqueous matrices.

3.2. Photophysical properties of OLPL materials

To understand the source of the long afterglow in doped crystals, we conducted relevant photophysical tests on doped crystals, host, and guest materials. First, we performed ultraviolet-visible (UV-vis) absorption spectroscopy tests, as shown in Fig. 2a. The UV-vis absorption peaks of each doped crystal essentially overlap with those of the corresponding monomer compounds. For doped crystals TPP: p-TPD and DPA: p-TPD, the absorption from 200–350 nm originates from the respective host matrices, TPP and DPA, and the absorption from 350–500 nm is attributable to the guest molecule, p-TPD; in the case of the doped crystal TPA: p-TPD, absorption from 240–370 nm is due to the host matrix TPA, and from 370–500 nm, it is due to the guest molecule, p-TPD.

Similarly, for doped crystal PB: p-TPD, the absorption in the range of 200–320 nm comes from PB, and the absorption in the range of 320–500 nm comes from p-TPD. This observation suggests that the UV-vis absorption of the doped crystals is merely a superposition of the host and guest compounds, without the formation of any new substances.

To further analyze the sources of afterglow in the doped crystals, we conducted tests on the fluorescence and phosphorescence emissions of the doped crystals, as well as the host and guest compounds. As shown in Fig. S4 (ESI†), the maximum fluorescence emission peak of the guest molecule p-TPD is located near 413 nm, and the fluorescence emission spectra of the four doped crystals closely match the fluorescence emission spectra of p-TPD. The maximum fluorescence emission peak exhibits a slight red shift to around 420 nm. The rigid environment provided by the host matrix suppresses the non-radiative deactivation of the excitons in p-TPD, enhancing the LPL performance of the doped material.[42,43] Concurrently, the potential interactions between the host and guest molecules contribute to a slight redshift in the fluorescence emission spectrum of the doped material relative to that of the guest molecules alone.[44-46] Such observations further reinforce the notion that the photophysical processes in doped crystals primarily originate from the internal guest molecule p-TPD. As shown in Fig. 2b, the phosphorescence emission spectra of
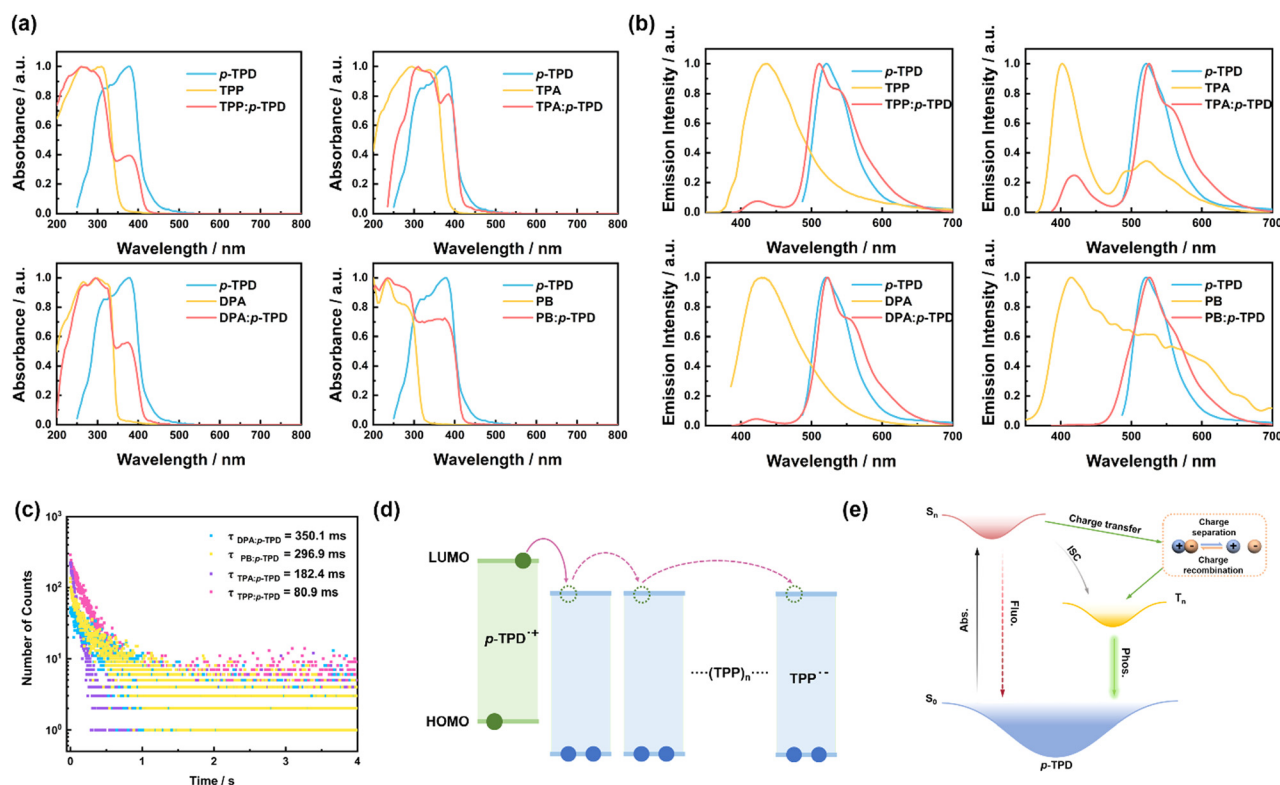

Fig. 2 (a) UV-vis absorption spectra of compounds p-TPD, TPP, TPA, DPA, PB, and doped crystals TPP: p-TPD, TPA: p-TPD, DPA: p-TPD, PB: p-TPD (Excitation: 365 nm), measured at room temperature under ambient conditions. (b) Phosphorescence emission spectra of compounds p-TPD, TPP, TPA, DPA, PB, and doped crystals TPP: p-TPD, TPA: p-TPD, DPA: p-TPD, and PB: p-TPD. (c) Phosphorescence emission attenuation spectra of the doped crystals. (d) Photophysical process of the doped-crystals. The measurement of the energies is exhibited in Table S1 (ESI†). (e) Based on the TPP: p-TPD doping system, charge separation can be induced through electron transfer under excitation, and (TPP)n (n ≥ 0) refers to several TPP molecules.

doped crystals TPP: *p*-TPD, TPA: *p*-TPD, DPA: *p*-TPD, and PB: *p*-TPD in the range of 470–700 nm closely match the phosphorescence emission spectra of the guest molecule *p*-TPD. Their corresponding maximum phosphorescence emission peaks are at 512 nm, 526 nm, 522 nm, and 527 nm, respectively, all of which are close to the emission peak of the guest molecule *p*-TPD at 523 nm. This reaffirms that the afterglow of the doped crystal primarily originates from the room temperature phosphorescence of the guest molecule *p*-TPD.

Fig. 2c and Fig. S5 (ESI†) exhibit the phosphorescence and fluorescence emission decay spectra of the doped crystals. As shown in Fig. S5 (ESI†), four doped crystals were analyzed using a double exponential decay model. This analysis reveals that the main and rapid components of the fluorescence emission lifetime are due to photoinduced electron transfer from the excited guest to the host module, leading to the formation of the CS state. The secondary and slower components are attributed to the conversion between singlet and triplet states. The fitting of the phosphorescence emission decay spectra reveals that the room temperature phosphorescence lifetimes of the doped crystals TPP: *p*-TPD, TPA: *p*-TPD, DPA: *p*-TPD, and PB: *p*-TPD are 80.9 ms, 182.4 ms, 350.1 ms, and 296.9 ms, respectively. These results indicate that the doped crystals exhibit excellent afterglow performance.

To further understand the luminescence mechanism of the host–guest doped system and the charge transfer between the host–guest materials, we analyzed the energy levels of the host–guest materials. We used cyclic voltammetry to obtain the oxidation potentials of the host and guest materials (Fig. S6, ESI†), determining their HOMO and LUMO energy levels. As shown in Fig. S7 (ESI†), the LUMO energy level of *p*-TPD is −2.27 eV, which is higher than the LUMO energy levels of the host compounds TPP, TPA, DPA, and PB (−2.46 eV, −2.47 eV, −2.51 eV, and −2.31 eV, respectively). Their energy levels are well-matched, indicating that *p*-TPD can function as a high-quality electron donor, while TPP, TPA, DPA, and PB can act as acceptors to achieve charge separation between host and guest molecules (Fig. 2d). Compared with inter-system crossing (ISC), the long-lived charge separation prolongs the transition time from the *p*-TPD singlet state of the guest molecule to the corresponding triplet state (Fig. 2e). Therefore, the doped system exhibits excellent luminescence performance.

To better reveal the impact of charge separation efficiency on the LPL performance, the photophysical processes of the four doped crystals under 365 nm excitation are detailed in Fig. S8 (ESI†). The energy diagram shows that the CS state has a higher energy value compared to the *p*-TPD triplet, confirming that the conversion from the CS state to the *p*-TPD triplet is feasible and that the prolonged charge separation extends the transition time. Additionally, analysis of the fluorescence emission decay spectrum in Fig. S5 (ESI†) provides the distribution ratio between *p*-TPD intersystem crossing and charge separation. This ratio varies among the doped crystals prepared with different host molecules, significantly affecting their phosphorescence lifetimes.[29] This variation underscores the importance of selecting appropriate host and guest combinations to optimize charge separation and enhance LPL performance.

3.3. "Paper-ink" encryption strategy

Considering the unique "host–guest pairing" relationship in the H–G doping system and taking advantage of its easy crystallization, we propose to construct an *in situ* anti-
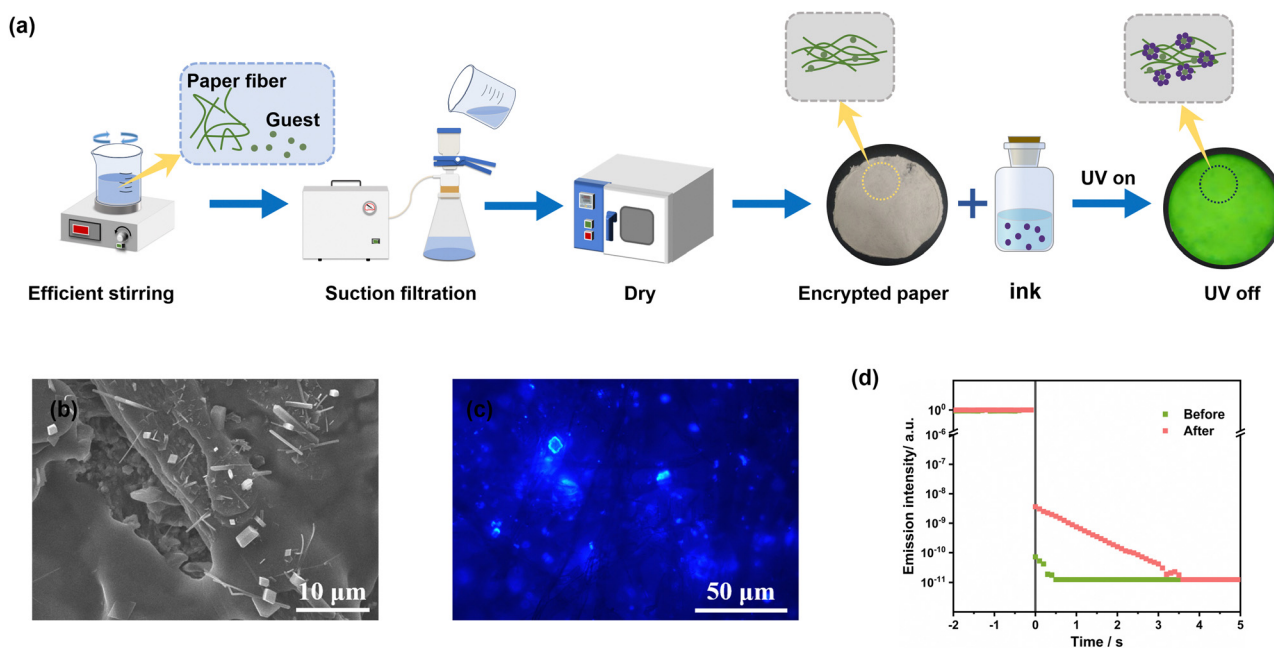

Fig. 3 (a) Preparation process diagram of the encryption paper and "paper-ink" encryption system. (b) SEM electron microscopy images of the encrypted paper. (c) Fluorescence microscopy images of the encrypted paper. (d) Semi-logarithmic plot of the emission decay profile of the encrypted paper before and after ink coating. (Sample-temperature: 300 K; excitation: 365 nm; excitation time: 2 s; excitation power: 10 mW.)
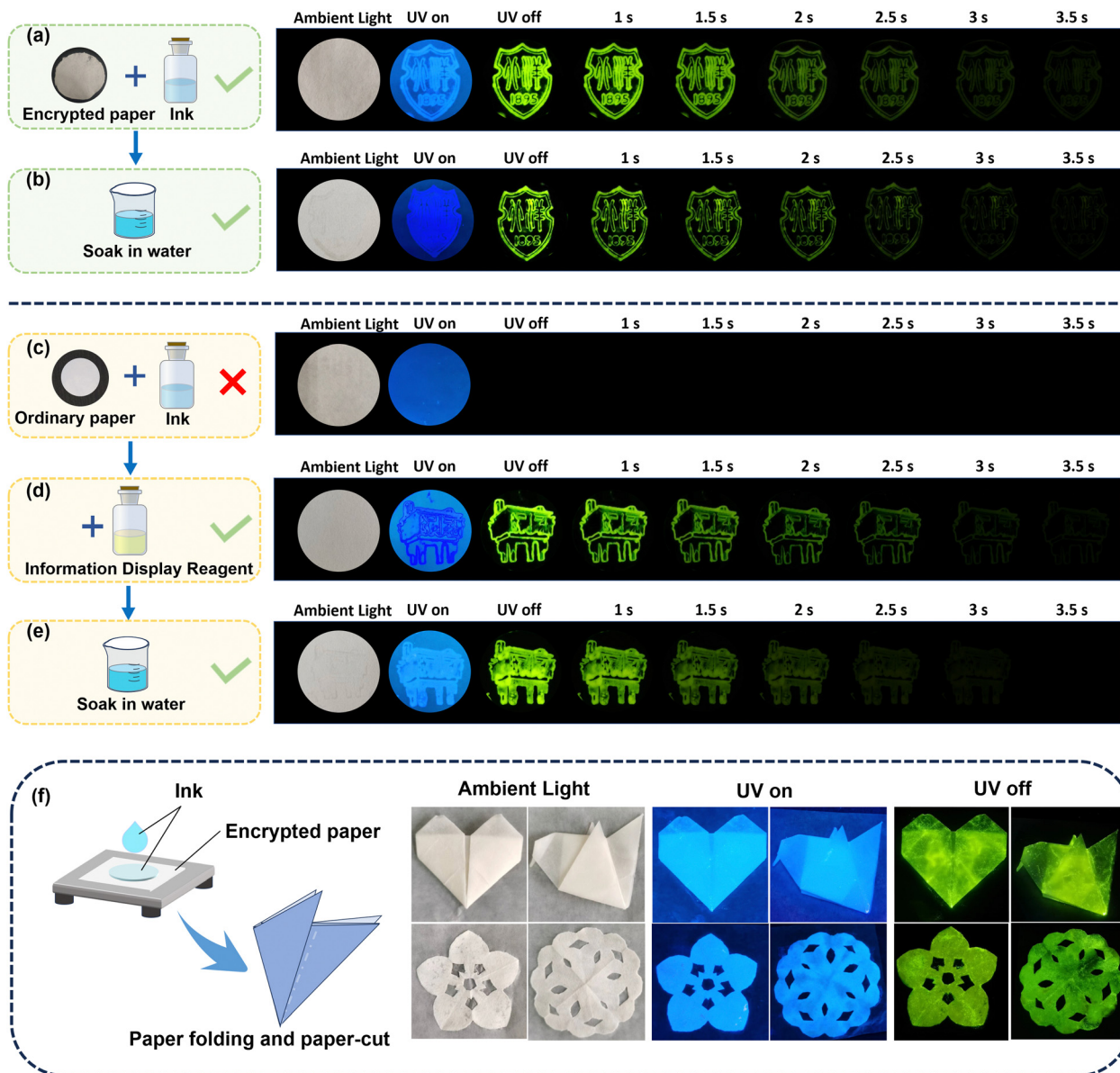
10946 | *J. Mater. Chem. C*, 2024, **12**, 10942–10949

This journal is © The Royal Society of Chemistry 2024

Fig. 4 (a) An afterglow photo of an encrypted paper and ink combination. (b) Photos of afterglow after soaking in water on the basis of (a). (c) Afterglow photos of ordinary paper combined with ink. (d) Photos of afterglow after applying information display reagent on the basis of (c). (e) Photos of afterglow after soaking in water on the basis of (d). (f) Paper folding and paper cuttings display of encrypted paper coated with ink.

counterfeiting encryption system. We have integrated the preparation process of doped crystals with papermaking technology to create encrypted paper that is paired specifically with this technology. Based on the materials embedded within the paper, the corresponding ink and information display reagent were developed to facilitate *in situ* anti-counterfeiting and encryption applications.

As depicted in Fig. 3a, the process involves thoroughly mixing *p*-TPD powder with pulp, followed by the preparation of paper cakes through filtration. These paper cakes are then compressed and dried to produce the corresponding encoded paper. SEM images (Fig. 3b and Fig. S9, ESI†) reveal numerous pores and gaps within the paper fibers, which facilitates the dispersion of doped crystals. Upon rapid volatilization of

dichloromethane in ink or information display reagent, the host material encapsulates the guest molecule *p*-TPD to form doped crystals, which are then dispersed within the pores of the paper fibers. Upon excitation by a light source, these doped crystals exhibit robust afterglow performance (Fig. 3c and d), thereby revealing the encoded information.

Fig. 4a–e displays two school emblem patterns printed with a special ink seal on encrypted paper. When excited with a 365 nm light source, green encrypted information becomes visible. For comparison, when the ink is applied to ordinary paper (Fig. 4c), the corresponding information remains hidden after excitation, showcasing excellent encryption characteristics. In order to further expand the application of this information encryption technology, we have also designed an "ink-inform-

ation display agent" encryption system that does not rely on special encryption paper. Fig. 4d demonstrates that encrypted information can be revealed by applying an information display reagent to the same paper used in Fig. 4c. Additionally, Fig. 4b and e display the afterglow images of two encryption methods after being soaked in water, demonstrating the strategy's stability in aquatic environments. The flexibility of the paper allows it to be manipulated into various shapes. As depicted in Fig. 4f, we folded the encrypted paper coated with special ink into the shapes of a heart and a paper kite, and also cut out two flower patterns. These folded and cut papers exhibit robust luminous performance, showcasing their potential application in anti-counterfeiting. Overall, this pairing information encryption strategy, derived from the doping system, demonstrates excellent encryption capabilities and potential application value, while maintaining robust encryption effects in water. It is expected to further advance OLPL materials in the information encryption field.

Conclusions

In summary, we have utilized *p*-TPD as the guest molecule, and TPP, TPA, DPA, and PB as the host molecules to construct a series of easily crystallizable doping systems. Through the use of surfactant molecules to form cavities, we successfully prepared a series of doped crystals with excellent dispersion and uniform particle size. The afterglow durations of doped crystals TPP: *p*-TPD, TPA: *p*-TPD, DPA: *p*-TPD, and PB: *p*-TPD are 4.5 s, 2.0 s, 3.0 s, and 2.2 s, respectively. Furthermore, based on the unique "H–G pairing" relationship and the facile crystallization characteristics in the host–guest doping system, we developed a "paper-ink" encryption strategy with *in situ* anti-counterfeiting. This approach allows encrypted paper and paired ink to fully display encrypted information, while ordinary paper treated with the ink does not display information without further processing with an information display reagent. Notably, the encrypted paper retains its encryption effectiveness even when exposed to water. We believe that this "paper-ink" encryption strategy holds great promise for advancing the application of organic long-persistent luminescence materials in the fields of information encryption and anti-counterfeiting.

Data availability

The data that support the findings of this study are available from the corresponding author upon reasonable request.

Conflicts of interest

The authors declare no conflict of interest.

Acknowledgements

Notes and references

1 Z. Li, S. Cao, Y. Zheng, L. Song, H. Zhang and Y. Zhao, *Adv. Funct. Mater.*, 2023, **34**, 2306956.
2 Y. Liang, M. Liu, T. Wang, J. Mao, L. Wang, D. Liu, T. Wang and W. Hu, *Adv. Mater.*, 2023, **35**, 2304820.
3 D. Y. Muleta, J. W. Song, W. H. Feng, R. T. Wu, X. Q. Zhou, W. Li, L. C. Wang, D. Z. Liu, T. Y. Wang and W. P. Hu, *J. Mater. Chem. C*, 2021, **9**, 5093–5097.
4 H. Xiao, D. S. Zheng, L. Y. Zhang, L. J. Xu and Z. N. Chen, *Adv. Funct. Mater.*, 2023, **33**, 2214241.
5 T. T. Wang, M. Liu, W. H. Feng, R. Cao, Y. J. Sun, L. C. Wang, D. Z. Liu, Y. Wang, T. Y. Wang and W. P. Hu, *Adv. Opt. Mater.*, 2023, **11**, 2202613.
6 Y. Lei, W. Dai, G. Li, Y. Zhang, X. Huang, Z. Cai and Y. Dong, *J. Phys. Chem. Lett.*, 2023, **14**, 1794–1807.
7 L. Kong, Y. Zhu, S. Sun, H. Li, F. Tao, F. Li, L. Wang and G. Li, *J. Mater. Chem. C*, 2023, **11**, 1960–1970.
8 J. Li, X. Li, G. Wang, X. Wang, M. Wu, J. Liu and K. Zhang, *Nat. Commun.*, 2023, **14**, 1987.
9 W. L. Zhou, Y. Chen, Q. Yu, H. Zhang, Z. X. Liu, X. Y. Dai, J. J. Li and Y. Liu, *Nat. Commun.*, 2020, **11**, 4655.
10 S. Li, Z. Y. Zhang, J. F. Lv, L. Li, J. Li and C. Li, *J. Mater. Chem. A*, 2023, **11**, 4957–4962.
11 T. Zhu, T. Yang, Q. Zhang and W. Z. Yuan, *Nat. Commun.*, 2022, **13**, 2658.
12 W. Zhao, Z. He and B. Z. Tang, *Nat. Rev. Mater.*, 2020, **5**, 869–885.
13 H. Shi, Z. An, P. Z. Li, J. Yin, G. Xing, T. He, H. Chen, J. Wang, H. Sun, W. Huang and Y. Zhao, *Cryst. Growth Des.*, 2016, **16**, 808–813.
14 Z. A. Yan and X. Ma, *ACS Mater. Lett.*, 2022, **4**, 2555–2561.
15 X. Q. Liu, W. B. Dai, J. J. Qian, Y. X. Lei, M. C. Liu, Z. X. Cai, X. B. Huang, H. Y. Wu and Y. P. Dong, *J. Mater. Chem. C*, 2021, **9**, 3391–3395.
16 L. Xiao, Y. Wu, J. Chen, Z. Yu, Y. Liu, J. Yao and H. Fu, *J. Phys. Chem. A*, 2017, **121**, 8652–8658.
17 S. Xu, W. Wang, H. Li, J. Zhang, R. Chen, S. Wang, C. Zheng, G. Xing, C. Song and W. Huang, *Nat. Commun.*, 2020, **11**, 4802.
18 D. Li, Y. Yang, J. Yang, M. Fang, B. Z. Tang and Z. Li, *Nat. Commun.*, 2022, **13**, 347.
19 L. Gu, H. Wu, H. Ma, W. Ye, W. Jia, H. Wang, H. Chen, N. Zhang, D. Wang, C. Qian, Z. An, W. Huang and Y. Zhao, *Nat. Commun.*, 2020, **11**, 944.

20 Z. Wu, J. Nitsch and T. B. Marder, *Adv. Opt. Mater.*, 2021, **9**, 2100411.

21 Y. Zuo, H. Yang, Y. Song, L. Jiang, W. Huang, Q. Jiang and B. Jiang, *ACS Appl. Polym. Mater.*, 2024, **6**, 2201–2209.

22 X. Fu, X. Zhang, C. Qian, Z. Ma, Z. Li, H. Jiang and Z. Ma, *Chem. Mater.*, 2023, **35**, 347–357.

23 C. Qian, X. Zhang, Z. Ma, X. Fu, Z. Li, H. Jin, M. Chen, H. Jiang and Z. Ma, *CCS Chem.*, 2024, **6**, 798–811.

24 S. Hirata, K. Totani, J. Zhang, T. Yamashita, H. Kaji, S. R. Marder, T. Watanabe and C. Adachi, *Adv. Funct. Mater.*, 2013, **23**, 3386–3397.

25 G. Qu, Y. Zhang and X. Ma, *Chin. Chem. Lett.*, 2019, **30**, 1809–1814.

26 T. Wang, M. Liu, J. Mao, Y. Liang, L. Wang, D. Liu, T. Wang and W. Hu, *Chin. Chem. Lett.*, 2024, **35**, 108385.

27 O. Bolton, K. Lee, H. J. Kim, K. Y. Lin and J. Kim, *Nat. Chem.*, 2011, **3**, 205–210.

28 B. Chen, W. Huang, X. Nie, F. Liao, H. Miao, X. Zhang and G. Zhang, *Angew. Chem., Int. Ed.*, 2021, **60**, 16970–16973.

29 M. Liu, J. Zong, L. Wang, D. Liu, T. Wang and W. Hu, *Adv. Opt. Mater.*, 2022, **10**, 2201684.

30 Y. X. Lei, J. F. Yang, W. B. Dai, Y. S. Lan, J. H. Yang, X. Y. Zheng, J. B. Shi, B. Tong, Z. X. Cai and Y. P. Dong, *Chem. Sci.*, 2021, **12**, 6518–6625.

31 M. Liu, D. Y. Muleta, Z. Y. Yu, L. C. Wang, D. Z. Liu, T. Y. Wang and W. P. Hu, *J. Mater. Chem. C*, 2022, **10**, 12249–12256.

32 Y. Zhang, J. Li, J. Zhao, X. Li, Z. Wang, Y. Huang, H. Zhang, Q. Liu, Y. Lei and D. Ding, *Angew. Chem., Int. Ed.*, 2024, **63**, e202313890.

33 J. Jiang, C. Hu, Y. Wang, L. Ma and J. Guo, *Mater. Today Chem.*, 2023, **30**, 101348.

34 Y. Huang, X. Zheng, Z. Yao, W. Lv, S. Xiang, Q. Ling and Z. Lin, *Chem. Eng. J.*, 2022, **444**.

35 J. Han, W. Feng, D. Y. Muleta, C. N. Bridgmohan, Y. Dang, G. Xie, H. Zhang, X. Zhou, W. Li, L. Wang, D. Liu, Y. Dang, T. Wang and W. Hu, *Adv. Funct. Mater.*, 2019, **29**, 1902503.

36 J. Song, D. Y. Muleta, W. Feng, Y. Song, X. Zhou, W. Li, L. Wang, D. Liu, T. Wang and W. Hu, *Dyes Pigm.*, 2021, **193**, 109501.

37 J. Cui, S. H. Ali, Z. Shen, W. Xu, J. Liu, P. Li, Y. Li, L. Chen and B. Wang, *Chem. Sci.*, 2024, **15**, 4171–4178.

38 B. Bhat, S. Pahari, J. S. I. Kwon and M. E. S. Akbulut, *Soft Matter*, 2023, **19**, 2231–2240.

39 W. Guan, X. Tang, W. Wang, Y. Lin and C. Lu, *Chem. Res. Chin. Univ.*, 2021, **37**, 116–122.

40 S. Kumari, S. Haider, R. Aggrawal, G. Sundar and S. K. Saha, *J. Mol. Liq.*, 2019, **294**, 111615.

41 S. Noguchi, K. Yamamoto and J. I. Kadokawa, *Int. J. Biol. Macromol.*, 2020, **157**, 680–686.

42 R. Kabe and C. Adachi, *Nature*, 2017, **550**, 384–387.

43 L. F. Bian, H. F. Shi, X. Wang, K. Ling, H. L. Ma, M. P. Li, Z. C. Cheng, C. Q. Ma, S. Z. Cai, Q. Wu, N. Gan, X. F. Xu, Z. F. An and W. Huang, *J. Am. Chem. Soc.*, 2018, **140**, 10734–10739.

44 H. Y. Gu, Y. Gao, Y. C. Duan, Y. Geng, L. Zhao, M. Zhang and Y. Wu, *J. Photochem. Photobiol., A*, 2020, **388**, 112195.

45 C. Gao, X. Li, Y. Qu, R. Dai, Z. Wang, H. Li and Z. Zhang, *J. Phys. Chem. C*, 2019, **123**, 8731–8739.

46 V. F. Traven, D. A. Cheptsov, J. I. Svetlova, I. V. Ivanov, C. Cuerva, C. Lodeiro, F. Duarte, S. F. Dunaev and V. V. Chernyshev, *Dyes Pigm.*, 2021, **186**, 108942.

This journal is © The Royal Society of Chemistry 2024

J. Mater. Chem. C, 2024, **12**, 10942–10949 | **10949**